**Atmospheric
Chemistry
and Physics**

Ship-borne FTIR measurements of CO and O₃ in the Western Pacific from 43° N to 35° S: an evaluation of the sources

T. Ridder[1], C. Gerbig[2], J. Notholt[1], M. Rex[3], O. Schrems[4], T. Warneke[1], and L. Zhang[5]

[1]Institute of Environmental Physics (IUP), University of Bremen, Otto-Hahn-Allee 1, 28359 Bremen, Germany
[2]Max Planck Institute (MPI) for Biogeochemistry, Hans-Knoell-Str. 10, 07745 Jena, Germany
[3]Alfred Wegener Institute for Polar and Marine Research (AWI) Potsdam, Telegrafenberg A43, 14473 Potsdam, Germany
[4]Alfred Wegener Institute for Polar and Marine Research (AWI) Bremerhaven, Am Handelshafen 12, 27570 Bremerhaven, Germany
[5]School of Engineering and Applied Sciences (SEAS), Harvard University, 29 Oxford Street, Cambridge, MA 02138, USA

Correspondence to: T. Ridder (tridder@iup.physik.uni-bremen.de)

Abstract. Carbon monoxide (CO) and ozone (O₃) have been measured in the Western Pacific (43° N to 35° S) during a ship campaign with Research Vessel Sonne in fall 2009. Observations have been performed using ship-based solar absorption Fourier Transform infrared spectrometry, flask sampling, balloon sounding, and in-situ Fourier Transform infrared analysis. The results obtained are compared to the GEOS-Chem global 3-D chemistry transport model for atmospheric composition. In general, a very good agreement is found between the GEOS-Chem model and all instruments. The CO and O₃ distributions show a comparable variability suggesting an impact from the same source regions.

Tagged-CO simulations implemented in the GEOS-Chem model make it possible to differentiate between different source processes and source regions. The source regions are verified with HYSPLIT backward trajectory calculations. In the Northern Hemisphere fossil fuel combustion in Asia is the dominant source. European and North American fossil fuel combustion also contribute to Northern Hemispheric CO pollution. In the Southern Hemisphere contributions from biomass burning and fossil fuel combustion are dominant; African biomass burning has a significant impact on Western Pacific CO pollution. Furthermore, in the tropical Western Pacific enhanced upper tropospheric CO within the tropical tropopause layer mainly originates from Indonesian fossil fuel combustion and can be transported into the stratosphere.

The source regions of the measured O₃ pollution are simulated with a tagged-O₃ simulation implemented in the GEOS-Chem model. Similar source regions compared to the tagged-CO simulations are identified by the model. In the Northern Hemisphere contributions from Asia, Europe, and North America are significant. In the Southern Hemisphere emissions from South America, south-east Africa, and Oceania significantly contribute to the measured O₃ pollution.

1 Introduction

Measurements of the global distribution of trace gases are indispensable to understand the dynamical and chemical processes in the atmosphere. Ground-based solar absorption Fourier Transform infrared (FTIR) spectrometry is a well established remote sensing technique for the observation of atmospheric trace gases (Rao, 1992; Notholt et al., 2003). Two global ground-based solar absorption FTIR networks (TCCON[1], NDACC[2]) are well established (Wunch et al., 2011; Kurylo, 1991). Besides observations from land-based FTIR stations, measurements have been performed in the Atlantic aboard Research Vessel (RV) *Polarstern* (Notholt et al., 2000; Velazco et al., 2005; Warneke et al., 2006). However, solar absorption FTIR measurements in the Pacific have not been previously performed. Here, we present the first solar absorption FTIR measurements in the Western Pacific complemented with in-situ observations.

---

[1]Total Carbon Column Observing Network (http://www.tccon.caltech.edu/)

[2]Network for the Detection of Atmospheric Composition Change (http://www.ndsc.ncep.noaa.gov/)

The tropical Western Pacific is considered to be the main region of troposphere to stratosphere transport (Holton et al., 1995; Fueglistaler et al., 2004, 2009). In the tropical warm pool (Yan et al., 1992) upwelling processes are enforced by high sea surface temperature and high air humidity. Thus, in this region tropospheric air has a relatively high probability of reaching the stratosphere (Notholt et al., 2005). The entry of tropospheric air into the stratosphere has a strong impact on stratospheric composition. However, the significance of various transport processes for the transport of different species is not yet fully understood.

The Western Pacific is of great interest with respect to trans-Pacific air mass transport. In the Northern Hemisphere (NH) the influence of the increasing anthropogenic pollution due to the fast economic growth in Asia and its impact on Northern Hemispheric air quality is studied (Zhang et al., 2008; Jacob et al., 2003). In the Southern Hemisphere (SH) biomass burning emissions and its global distribution are analyzed (Andreae et al., 2001; Thompson et al., 2001).

In the present study we concentrate on the evaluation of the source processes and source regions of carbon monoxide (CO) and ozone (O_3) in the Western Pacific during a ship campaign with RV *Sonne* in fall 2009. CO is produced during fossil fuel combustion, biomass burning, and oxidation of methane (CH_4) and other non-methane hydrocarbons (NMHC). The major sink of CO is the oxidation by OH. The lifetime of CO ranges from weeks to several months. According to the 2007 IPCC (Intergovernmental Panel on Climate Change) report (Solomon et al., 2007) O_3 is the fourth most important contributor to global warming. The main tropospheric source processes of O_3 are the photochemical oxidation of CO, CH_4, and volatile organic compounds (VOC) in the presence of nitrogen oxides (NO_x) and hydrogen oxides (HO_x). The main sink of O_3 is photochemical degradation forming OH.

In this study measurements of CO and O_3 in the Western Pacific ($43°$ N to $35°$ S) are presented. Since observations of CO and O_3 are rare in the Western Pacific, these measurements aim to contribute to a better understanding of the composition of the Western Pacific atmosphere. The observations are compared to model simulations which test the current understanding of Western Pacific composition. Furthermore, this study provides an evaluation of the source processes and source regions of Western Pacific CO and O_3 pollution to improve the knowledge of the contribution of these sources.

In Sect. 2 the underlying ship campaign is introduced. In Sect. 3 the instrumental setup and the model are described. This includes remote sensing and in-situ observations. In Sect. 4 results from the ship campaign and a model comparison are presented and discussed. Sources of CO and O_3 pollution are analyzed in Sect. 5.
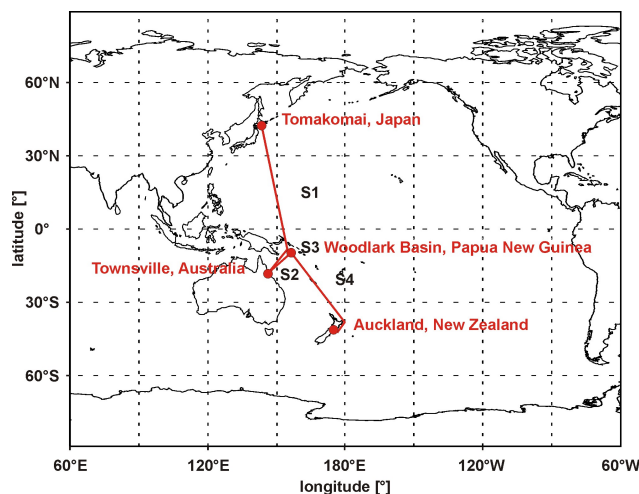

Fig. 1. Overview of the ship campaign with RV *Sonne* in the Western Pacific between 9 October 2009 and 5 December 2009 from Tomakomai, Japan, to Auckland, New Zealand, divided into four sections (S1–S4) according to Table 1. The red line indicates the approximate ship track. Section S1 is further described in Krüger and Quack (2012).

2   Ship campaign

Measurements of CO and O_3 concentrations in the Western Pacific have been performed aboard RV *Sonne* in fall 2009. The campaign was performed as a north-to-south transit starting in Tomakomai, Japan, on 9 October 2009 and ending in Auckland, New Zealand, on 5 December 2009. An overview of the campaign is shown in Fig. 1. For a better visualization and interpretation of the dataset the transit was split into four sections according to Table 1. Section S1 was part of the TransBrom (very short lived bromine compounds in the ocean and their transport pathways into the stratosphere) campaign, while cruise sections S2–S4 were part of the SO-203 campaign. Both campaigns were organized by the Leibniz Institute of Marine Sciences at the University of Kiel (IFM-Geomar), Kiel, Germany. For a further description of the campaigns the reader is referred to Krüger and Quack (2012), Quack and Krüger (2010), and http://www.rf-bremen.de/.

3   Method

3.1   Solar absorption FTIR spectrometry

Solar absorption Fourier Transform infrared (FTIR) spectrometry was performed aboard RV *Sonne* using a Bruker IFS 120M spectrometer upgraded with new electronics equivalent to the newer Bruker IFS 125M instrument. The experimental setup for ship-borne measurements is described in Notholt et al. (2000). Solar absorption FTIR spectra were recorded in the spectral region between $700\,cm^{-1}$ and

Table 1. Description of the four sections (S1–S4) of the ship campaign with RV *Sonne* according to Fig. 1. Section S1 is further described in Krüger and Quack (2012).

Section	Location	Latitude	Date
S1	Tomakomai, Japan–Townsville, Australia	43° N–20° S	9 Oct 2009–24 Oct 2009
S2	Townsville, Australia–Woodlark Basin, Papua New Guinea	20° S–10° S	26 Oct 2009–30 Oct 2009
S3	Woodlark Basin, Papua New Guinea	10° S	30 Oct 2009–28 Nov 2009
S4	Woodlark Basin, Papua New Guinea–Auckland, New Zealand	10° S–35° S	28 Nov 2009–5 Dec 2009
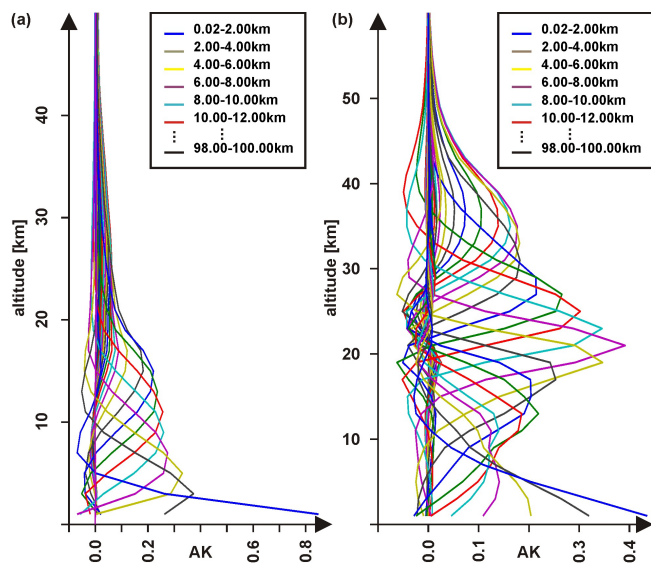
Fig. 2. Representative averaging kernels of the FTIR **(a)** CO retrieval and **(b)** O_3 retrieval. The colored lines indicate the sensitivity and resolution of each individual layer.

15 780 cm^{-1} with a maximum resolution of 0.005 cm^{-1}. The meteorological conditions were permanently monitored to minimize the influence of clouds on solar absorption FTIR spectra. Small unavoidable intensity fluctuations caused by thin clouds were corrected using the method described by Ridder et al. (2011).

The retrieval of trace gas concentrations from solar absorption FTIR spectra was performed using the SFIT-2 (Spectral Least Squares Fitting) software developed at the NASA Langley Research Center and the National Institute for Water and Atmospheric Research in New Zealand (Rinsland et al., 1998). A priori pressure and temperature profiles were obtained from the NCEP (National Center for Environmental Prediction, http://www.ncep.noaa.gov/) database. Meteorological observations from radiosondes, which were launched four times per day during cruise section S1 (Krüger et al., 2012), were delivered to the World Meteorological Organization (WMO) global database to be assimilated into the NCEP database. Spectral line parameters were taken from the HITRAN2004 (high-resolution transmission molecular absorption) database including the 2006 updates for H_2O. A priori profiles were kept constant for

the entire campaign and were extracted from the WACCAM model (Garcia et al., 2007) at the location of the NDACC and TCCON station in Wollongong, Australia (34° S, 151° E). CO was retrieved simultaneously in three microwindows (2057.70 cm^{-1}–2057.91 cm^{-1}, 2069.55 cm^{-1}–2069.72 cm^{-1}, 2157.40 cm^{-1}–2159.20 cm^{-1}) including the interfering gases H_2O, N_2O, and O_3. O_3 was retrieved in a single microwindow (1000 cm^{-1}–1005 cm^{-1}) with a simultaneous fit of H_2O.

The sensitivity of the retrieval is expressed by the averaging kernels (AK) showed in Fig. 2. The height of each individual averaging kernel is an indicator for the sensitivity of the corresponding layer, while the width is an indicator for the vertical resolution (Rodgers, 2000). The degree of freedom (DOF) for signal is an expression for the number of independent layers in the retrieval (Rodgers, 1990). CO is mainly sensitive in the troposphere with a DOF between 3.0 and 4.0. O_3 is sensitive in the troposphere and stratosphere with a DOF of up to 5.0.

3.2 In situ data

3.2.1 FTIR analyzer

Surface concentrations of CO were continuously measured aboard RV *Sonne* with a FTIR in-situ trace gas analyzer (Griffith et al., 2010; Esler et al., 2000) developed and constructed by the Centre for Atmospheric Chemistry at the University of Wollongong. The system uses a low-resolution FTIR spectrometer (1 cm^{-1}) to quantify the volume mixing ratios (vmr) of CO, CH_4, CO_2, N_2O, and $\delta^{13}C$ in CO_2. The FTIR spectrometer measures the transmission spectrum of an air sample within a multipass White cell (White, 1942). The transmission spectrum is then analyzed with the Multiple Atmospheric Layer Transmission (MALT) nonlinear least squares-fitting software (Griffith, 1996, 2002). A detailed description of the instrument can be found in Griffith et al. (2010).

3.2.2 Flasks

Approximately 30 flasks were taken aboard RV *Sonne* and were analyzed by the Max Planck Institute for Biogeochemistry in Jena, Germany. Air samples were dried during collection using magnesium perchlorate and compressed to 2 bar absolute yielding a sample size of 2 l. Concentrations
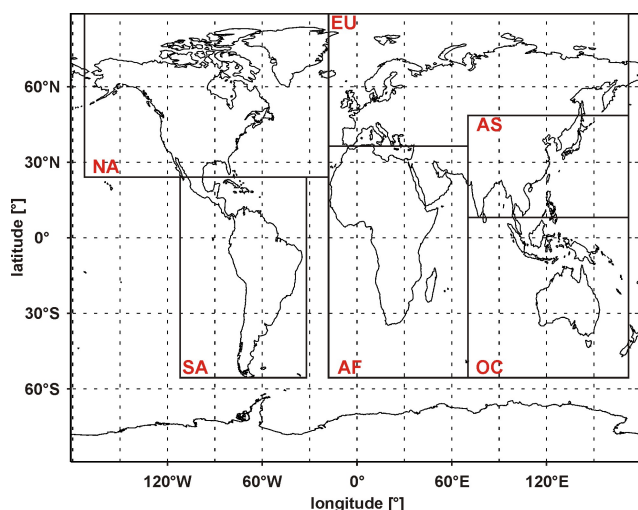
Fig. 3. Tropospheric source regions of the GEOS-Chem tagged-CO simulation. NA: North America, EU: Europe, AS: Asia, SA: South America, AF: Africa, and OC: Oceania.

of CO, CO_2, CH_4, N_2O, SF_6, $\delta^{13}C$ in CO_2, and $\delta^{18}O$ in CO_2 were determined by gas chromatography and mass spectrometry. For measurement accuracy the reader is referred to http://www.bgc.mpg.de/service/iso_gas_lab/gas_lab/techniques_results/index.shtml and to http://www.bgc.mpg.de/service/iso_gas_lab/techniques_results/irm_eams.shtml.

3.2.3 Balloon sondes

Daily O_3-sondes (Science Pump Corporation ECC-6A) were launched during cruise section S1. Meteorological conditions obtained from radiosonde observations during S1 (Krüger and Quack, 2012) were delivered to the WMO global database.

3.3 GEOS-Chem

CO and O_3 concentrations in the Western Pacific were simulated using version v8-02-04 of the global 3-D chemistry transport model GEOS-Chem for atmospheric composition. The model is described in Bey et al. (2001b). GEOS-Chem is driven by GEOS-5 (Rienecker et al., 2008) assimilated meteorological observations from the NASA Global Modeling and Assimilation Office (GMAO). Model profiles were sampled along the ship track every three hours with a horizontal resolution of $2° \times 2.5°$ and a vertical resolution of 47 layers using the GEOS-Chem full chemistry simulation. Model results for carbon monoxide (CO) are scaled by a factor $\beta = 1.2$ to balance a consistent low bias in the GEOS-Chem simulation (Kopacz et al., 2010).

In order to identify CO sources from different source regions the tagged-CO simulation (Duncan et al., 2007) implemented in the GEOS-Chem model is applied using monthly mean OH concentrations from a previous full-chemistry run

as the primary CO sink. The tagged-CO simulation calculates source processes of CO such as fossil fuel combustion, biomass burning, biofuel, oxidation of CH_4, and volatile organic compounds (VOC) from various source regions. An overview of the standard source regions within the tagged-CO simulation is shown in Fig. 3. Similar approaches have been previously used by Bey et al. (2001a); Staudt et al. (2001).

In order to identify the source regions of the measured O_3 pollution, the tagged-O_x simulation implemented in the GEOS-Chem model has been used. The tagged-O_x simulation calculates the contributions of the trace regions in Fig. 3 using daily production rates and loss frequencies of odd oxygen ($O_x = O_3 + NO_2 + 2 \times NO_3 + HNO_3 + PAN + HNO_4 + 3 \times N_2O_5$). In the following tagged-O_x will be referred to as tagged-O_3 since ozone generally represents more than 95 % of odd oxygen. Model output was generated for ozone production in the lowest five layers of the model; this simulation provides information about the direct production of O_3 over the continent and hints at the origin of the pollution. However, the simulation does not account for a secondary production of ozone from ozone precursors in the free troposphere and, thus, underestimates the simulated contributions. Similar approaches have previously been used by Sauvage et al. (2007); Li et al. (2002); Liu et al. (2002).

3.4 Intercomparison

CO and O_3 concentrations from different instruments and from model simulations are compared in this study. Thus, it is necessary to take the different characteristics of the different observing systems into account (Rodgers and Connor, 2003; Palm et al., 2005). In-situ observations and model results are generally compared directly to each other. However, when comparing solar absorption FTIR profiles to GEOS-Chem model profiles, the characteristics of the FTIR retrieval have to be considered; the FTIR measurements do not provide simple measurements of the true state x, rather they provide the estimated state of the atmosphere $\hat{x}$ which can be derived from the weighted contribution of the true state and the a priori state x_a (Rodgers, 1990, 2000).

$$\hat{x} = x_a + A(x - x_a) + \epsilon_x \tag{1}$$

In Eq. (1) ϵ_x represents the error in $\hat{x}$ and A represents the averaging kernel matrix. To account for the characteristics of the FTIR retrieval, model profiles x_m are expressed as smoothed model profiles x_s retrieved with the resolution of the FTIR instrument in the absence of the error term.

$$x_s = x_a + A(x_m - x_a) \tag{2}$$

The GEOS-Chem model simulates CO and O_3 concentrations only in the troposphere. For the smoothing in Eq. (2) a full model profile is needed. The standard method for handling this problem is to create a composite profile by

combining the modeled tropospheric profile with the FTIR a priori profile above the tropopause[3].

CO total column concentrations calculated from the FTIR profiles and the smoothed composed model profiles are compared directly to each other in Sect. 4. Although the model does not reproduce stratospheric variations, the error in the column is negligible since more than 90 % of atmospheric CO is located in the troposphere. Furthermore, the CO retrieval is not very sensitive in the stratosphere (Fig. 2a) and mainly reproduces the a priori profile.

O_3 tropospheric columns are calculated from the FTIR profiles and are directly compared to the raw model tropospheric columns and the tropospheric columns derived from the sondes following the approach in Schneider et al. (2008). For the calculation of the FTIR tropospheric columns the model tropopause height is used.

4   Results and discussion

4.1   CO

Figure 4 shows the CO distribution during the four sections of the ship campaign with RV *Sonne*. Each plot in Fig. 4 is divided into the four cruise sections described in Table 1; sections S1, S2, and S4 are plotted over latitude, and section S3 is displayed over time. Figure 4a shows the CO surface volume mixing ratio measured with the FTIR in-situ analyzer compared to flask measurements and the GEOS-Chem model. To exclude contamination by the ship plume, the FTIR in-situ data is filtered by wind direction ($\alpha \geq 30°$) and relative wind speed ($v_{rel} \geq 5\,\mathrm{m\,s^{-1}}$). Individual peaks in the dataset may originate from nearby ship traffic. In general, CO concentrations from flask measurements and the FTIR in-situ analyzer agree well. Small-scale variations resolved by the FTIR in-situ analyzer are not reproduced by the model. The cause of the overestimation in the beginning of cruise section S1 is discussed in Sect. 5.1. Figure 4b displays the CO total column amounts derived from the solar absorption FTIR spectrometer and the GEOS-Chem model. The model reproduces the main features in the CO total column distribution. Figures 4c–e show the CO volume mixing ratio (vmr) profiles from panel c: the solar absorption FTIR spectrometer, panel d: the GEOS-Chem model smoothed with the FTIR averaging kernels, and panel e: the raw GEOS-Chem model. The agreement between the model profiles and the FTIR profiles is good. Additionally, the model tropopause height (TPH) is shown. A typical equatorial TPH of around 17 km is simulated as well as the typical tropopause height decrease at 30° N and 30° S, respectively. The simulated

---

[3]The tropopause is defined as the lowest level at which the temperature lapse rate decreases to $2\,\mathrm{K\,km^{-1}}$ or less, and the lapse rate averaged between this level and any level within the next 2 km does not exceed $2\,\mathrm{K\,km^{-1}}$ (WMO definition).

Table 2. CO pollution events (PE1–PE4) during the ship campaign with RV *Sonne* in the Western Pacific (TPH: tropopause height, LT: lower troposphere).

Pollution	Section	Latitude	Altitude
PE1	S1	43° N–20° N	0 km-TPH
PE2	S1–S2	10° S–20° S	0 km, 4–8 km
PE3	S3	9° S	12–17 km
PE4	S3–S4	9° S–20° S	LT

TPH coincides with the measured TPH from radiosonde observations during cruise section S1 (Krüger et al., 2012).

Figure 4 especially reveals the impact of several pollution events (PE). At the location corresponding to the beginning of cruise section S1 the GEOS-Chem model simulates a strong pollution event from the surface up to the tropopause (PE1). It was not possible to observe the pollution by the solar absorption FTIR spectrometer due to bad measurement conditions during that time period caused by the typhoon Melor. FTIR in-situ data, however, does not support polluted surface air simulated by the GEOS-Chem model and shows, on the contrary, clean surface air of about 60 ppb. Between sections S1 and S2 around 20° S all instruments show a further CO enhancement (PE2). Surface volume mixing ratios suggest local pollutants in the harbor of Townsville, Australia, at 19° S. Local pollutants are captured by the model but underestimated due to resolution effects. Total column concentrations suggest the influence of a further CO source in this region since the concentrations start to rise at 10° S. Profiles obtained by solar absorption FTIR spectrometry reveal enhanced CO concentrations in 4–8 km altitude to be the main contributor to the increased total column amounts. This mid tropospheric CO pollution is reproduced but underestimated by the GEOS-Chem model. Within section S3 at 10° S the solar absorption FTIR instrument and the GEOS-Chem model reveal a CO band in the upper troposphere (PE3). FTIR and smoothed model profiles, both reveal the pollution at similar heights between 6–12 km altitude. Thus, the actual height of the CO pollution can be determined from the raw model output, which pictures PE3 in 12–17 km altitude within the tropical tropopause layer (TTL). Based on Fueglistaler et al. (2009) it can be assumed that CO pollution within the TTL is transported by radiative heating into the stratosphere in this area. Between section S3 and S4 a fourth CO pollution event (PE4) occurs. Surface volume mixing ratios and model profiles, both picture PE4 as a near surface event. Solar absorption FTIR measurements also suggest the impact of mid tropospheric CO pollution.

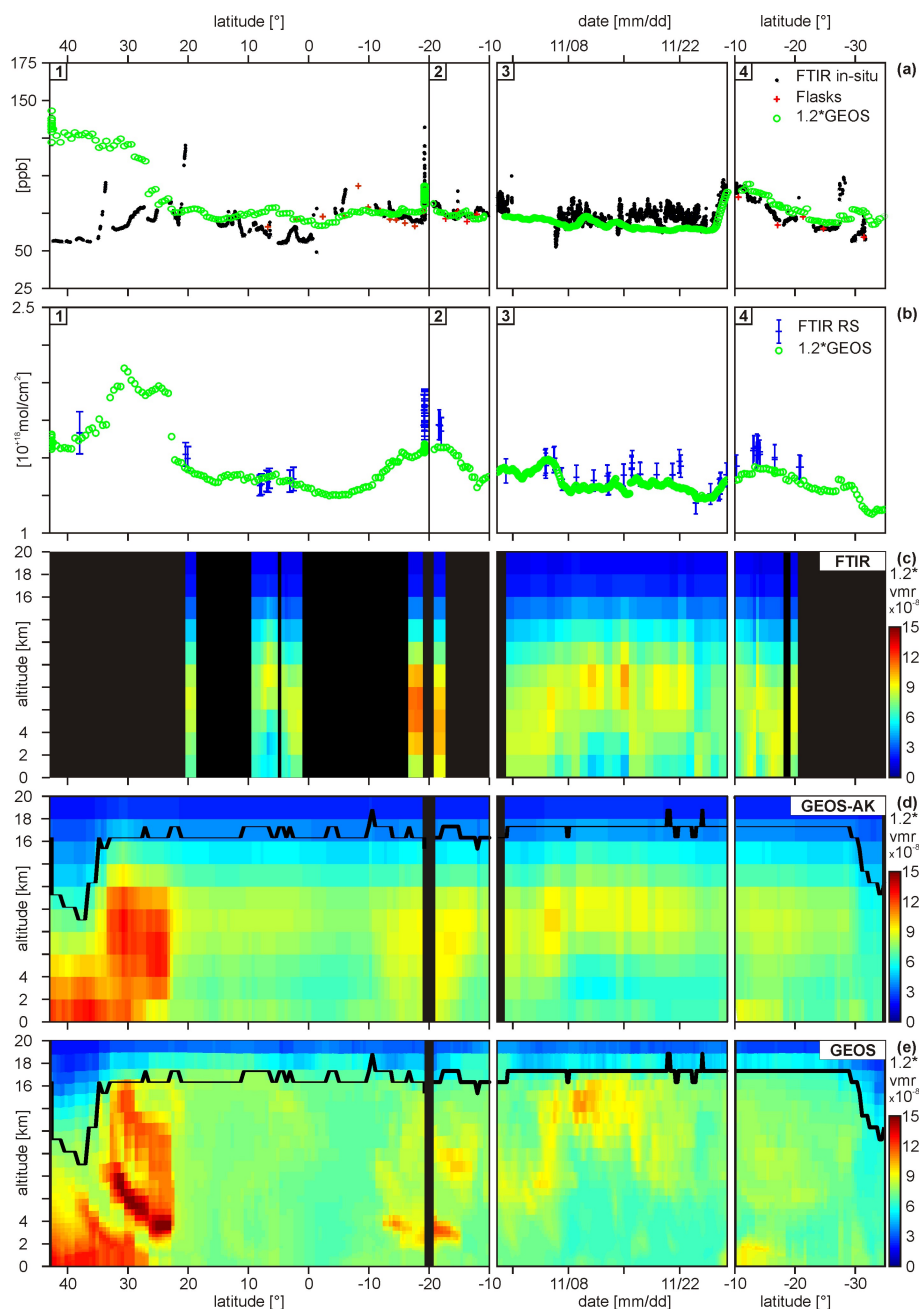An overview of the four pollution events discussed in this section is presented in Table 2.

Fig. 4. CO distribution during the four sections of the ship campaign with RV *Sonne* in the Western Pacific; **(a)** surface volume mixing ratios obtained from FTIR in-situ measurements (black dots) and flask sampling (red crosses) compared to the GEOS-Chem model (green circles), **(b)** total column concentrations obtained from solar absorption FTIR measurements (blue markers, the error bars represent the theoretical uncertainty in the FTIR retrieval) compared to the GEOS-Chem model (green circles), **(c)** solar absorption FTIR profiles, **(d)** GEOS-Chem profiles smoothed with FTIR averaging kernels, **(e)** raw GEOS-Chem profiles. The black lines in **(d)** and **(e)** represent the model tropopause height.

4.2 O₃

Figure 5 shows the O₃ distribution during the four sections of the ship campaign with RV *Sonne* (Table 1). Figure 5a displays the tropospheric partial column concentrations of

O₃ derived from the solar absorption FTIR spectrometer in comparison to tropospheric columns derived from O₃-sondes and the GEOS-Chem model. Figures 5b–e show the O₃ volume mixing ratio profiles from panel b: the FTIR spectrometer, panel c: the GEOS-Chem model smoothed with FTIR
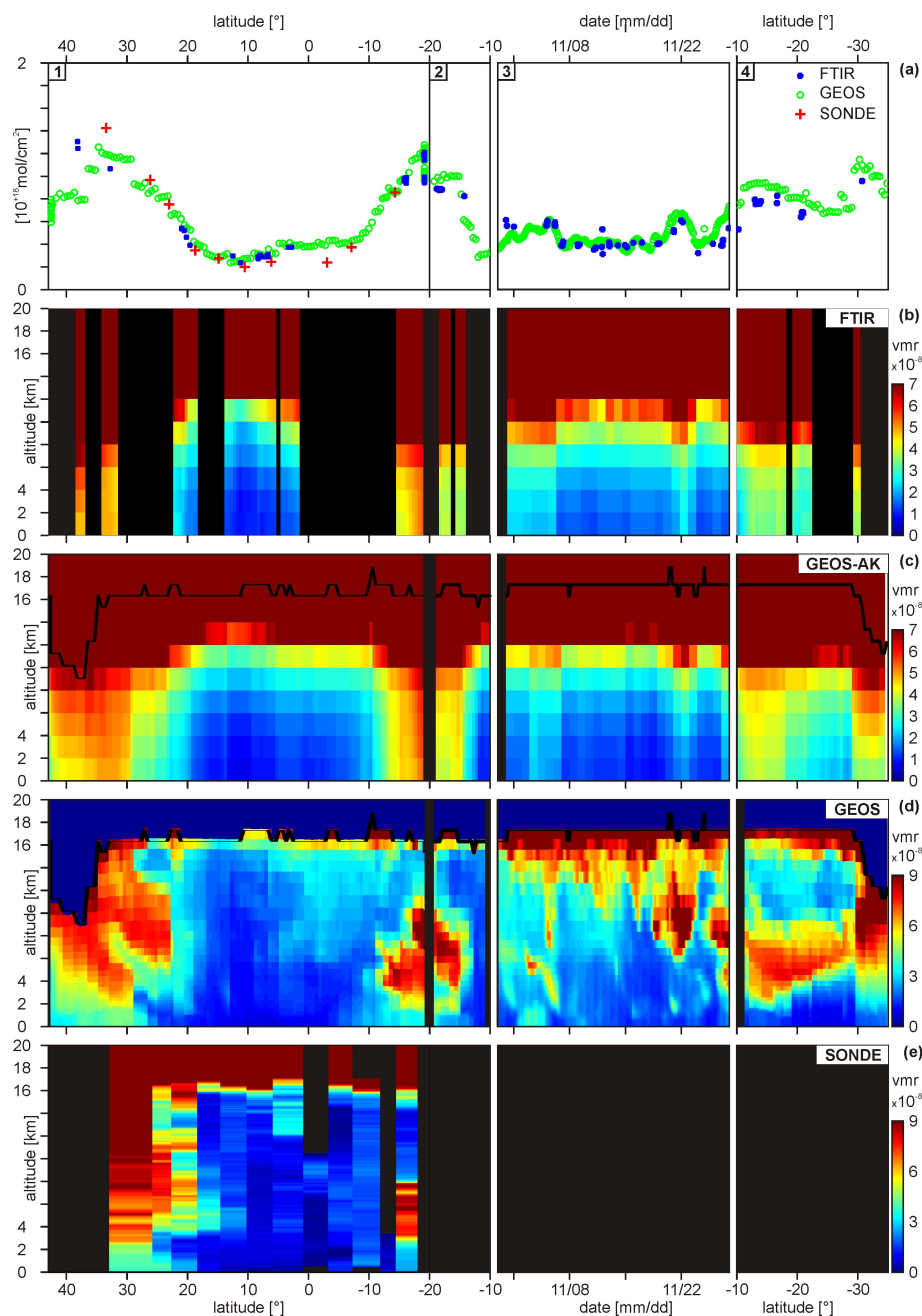
Fig. 5. O$_3$ distribution during the four sections of the ship campaign with RV *Sonne*; **(a)** tropospheric columns obtained from solar absorption FTIR measurements (blue dots) and O$_3$-sonde measurements (red crosses) compared to the GEOS-Chem model (green circles), **(b)** solar absorption FTIR profiles, **(c)** GEOS-Chem profiles smoothed with FTIR averaging kernels, **(d)** raw GEOS-Chem profiles, **(e)** O$_3$-sonde profiles. The black lines in **(c)** and **(d)** represent the model tropopause height.

averaging kernels, panel d: the raw GEOS-Chem model, and panel e: the O$_3$-sondes (only cruise section S1). The overall agreement between the model and the observations is very good and the model reproduces the variability as well as the magnitude of the measurements.

In general, the O$_3$ distributions are quite similar to the CO distributions in Fig. 4 and all four pollution events (Ta-

ble 2) can also be identified in the O$_3$ distributions. PE1 within cruise section S1 is this time also captured by the solar absorption FTIR spectrometer[4] and the O$_3$-sondes. Mid

---

[4]The weather conditions in the beginning of the ship campaign partly allowed to measure not more than one to two spectra during the day. For those spectra the spectral region from $700\,\mathrm{cm}^{-1}$ to $1350\,\mathrm{cm}^{-1}$ was preferred against other spectral regions. This

tropospheric pollution (PE2) between cruise sections S1 and S2 is clearly observed by the FTIR spectrometer, the GEOS-Chem model, and the O$_3$-sondes. Upper tropospheric pollution in the Woodlark Basin (PE3) can not be resolved by the FTIR spectrometer since high O$_3$ concentrations are convolved from the stratosphere into the troposphere by the averaging kernels and overlay the tropospheric O$_3$ signal. However, raw model volume mixing ratio profiles show enhanced upper tropospheric O$_3$. PE4 is seen in the mid troposphere rather than at the surface. Furthermore, enhanced O$_3$ at the end of cruise section S4 between 26° S and 32° S is observed.

Due to the fact that the O$_3$ and CO distributions are similar, one can hypothesize that the source regions of the observed CO and O$_3$ pollution are related. This aspect will be discussed in more detail in Sect. 5.

5 Sources of CO and O$_3$

To identify the source processes and source regions of the measured CO and O$_3$ pollution in the Western Pacific, the GEOS-Chem model tagged tracer simulations for CO (Sect. 5.1) and O$_3$ (Sect. 5.4) are applied. Model tagged tracer simulations deliver the contributions of various source processes and source regions to the modeled Western Pacific pollution. In addition, backward trajectory calculations combined with firemaps (Sect. 5.2) and solar absorption Fourier Transform infrared HCN measurements (Sect. 5.3) are presented. Trajectory studies reveal the transport pathways of Western Pacific air parcels. HCN measurements and firemaps show the impact of biomass burning. The discussion focuses on emissions from fossil fuel combustion and biomass burning.

5.1 Tagged-CO simulation

To identify the contributions of different source processes and source repetitive regions to the measured CO pollution (Fig. 4) in the Western Pacific with the GEOS-Chem model, CO is decomposed into tagged tracers as described in Sect. 3.3. The sum of all tagged tracers reproduces closely the results from the standard full-chemistry simulation shown at the top of Fig. 6. Below, the main CO contributions (with contributions > 10 %) calculated with the tagged-CO simulation are presented as the relative contributions to the total CO concentration.

During PE1 the main contribution is from Asian fossil fuel combustion (ASFF) (≈40 %). European fossil fuel combustion (EUFF) (≈15 %) and North American fossil fuel combustion (NAFF) (≈10 %) contribute to lower tropospheric CO pollution between 43° N and 30° N. The impact of European and North American CO emissions on the Western Pacific and their transport pathways have been discussed

spectral region includes the O$_3$ microwindow but not the CO microwindows.
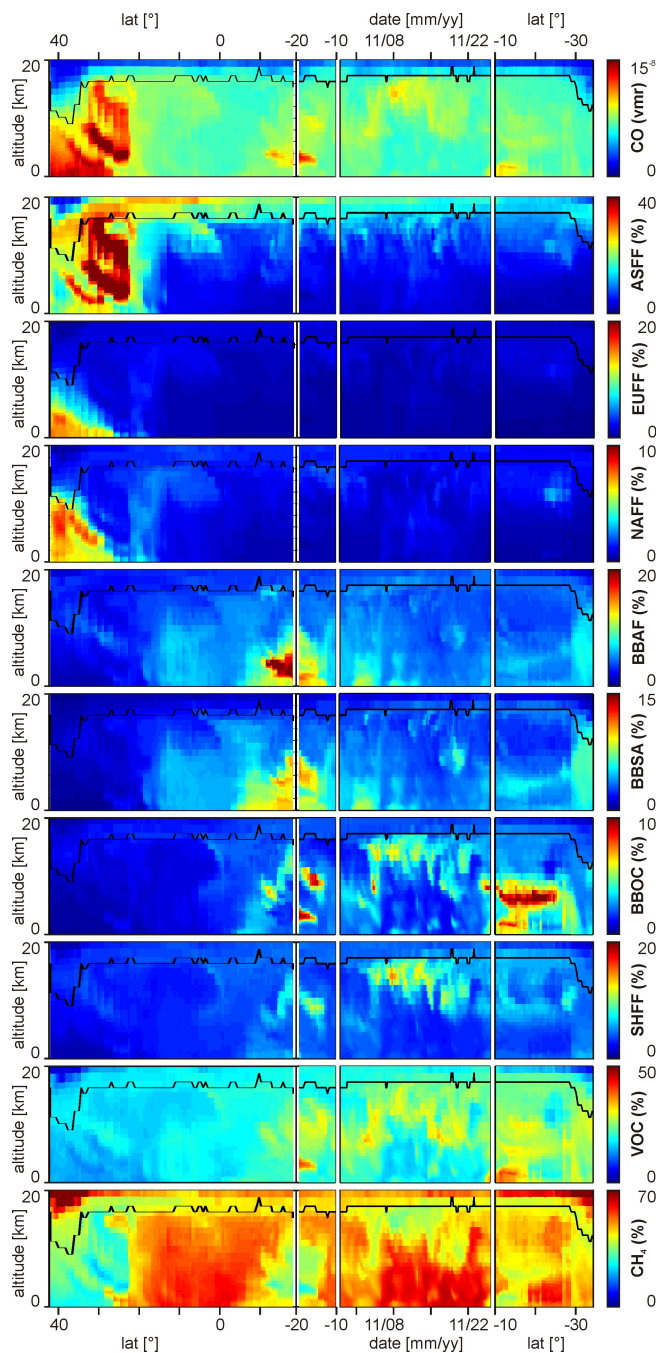

Fig. 6. Total CO vertical profiles (top) simulated with the GEOS-Chem tagged-CO simulation and relative contributions of various tracers from different trace regions (ASFF: Asian fossil fuel, EUFF: European fossil fuel, NAFF: North American fossil fuel, BBAF: African biomass burning, BBSA: South American biomass burning, BBOC: biomass burning from Oceania, SHFF: Southern Hemispheric fossil fuel, VOC: volatile organic compounds, CH$_4$: oxidation of methane). The black line in each graph indicates the model tropopause height.
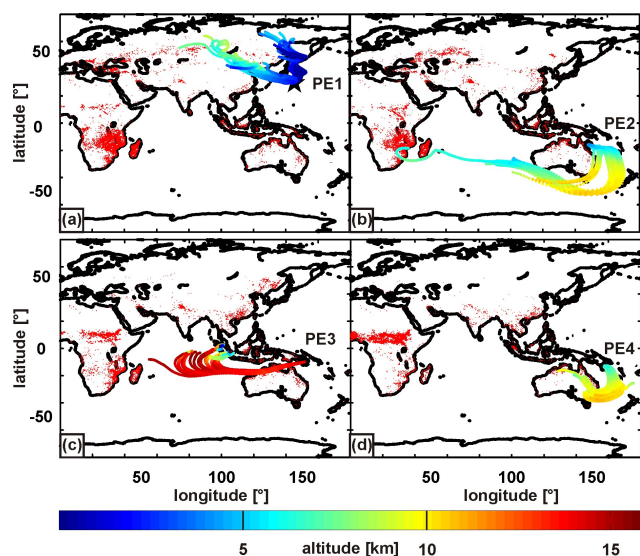
Fig. 7. HYSPLIT backward ensemble (120 h) and single (315 h) trajectories calculated at one representative altitude for the four characteristic locations; **(a)** PE1, **(b)** PE2, **(c)** PE3, and **(d)** PE4. The altitude of the trajectories is expressed by the color bar. MODIS fire counts (red dots) are displayed to picture the impact of biomass burning.

in Jaeglé et al. (2003); Bey et al. (2001a). The GEOS-Chem model simulates contributions from ASFF, EUFF, and NAFF to the surface layer, whereas the FTIR in-situ analyzer suggest clean air concentrations of 60 ppb. This suggests a problem with the representation of the boundary layer in the model, which seems to mix free tropospheric air into the boundary layer too readily in this meteorological situation.

The main contributions to the pollution close to Australia (PE2) are from African biomass burning (BBAF) (>20 %). Significant contributions (≈15 %) originate from South American biomass burning (BBSA). Small contributions from biomass burning from Oceania (OCBB) (≈10 %) are also apparent. The upper tropospheric pollution PE3 mainly originates from fossil fuel combustion in the Southern Hemisphere (SHFF) (≈15 %). Biomass burning from the Oceania region contributes around 10 % to the total PE3 pollution. PE4 pollution mainly originates from biomass burning in Oceania (≈10 %). The most dominant background source is oxidation of methane (CH$_4$), which contributes up to 70 % in unpolluted regions. The strong variability in CH$_4$ relative contributions is mainly due to the variability in all other contributions. The absolute CH$_4$ contributions (not shown) ranges between 25 ppb and 35 ppb. Oxidation of volatile organic compounds (VOC) provides a background of around 20 % in unpolluted regions, but is also responsible for part of the CO variability in the Southern Hemisphere.

5.2 Backward trajectories

In order to verify the source regions of the measured CO pollution, backward trajectories were calculated with the NOAA HYSPLIT (National Oceanic and Atmospheric Administration Hybrid Single Particle Lagrangian Integrated Trajectory) model (Draxler and Hess, 1997, 1998) at the four characteristic points PE1, PE2, PE3, and PE4 (Fig. 7). For the calculations the NCEP-GDAS meteorological assimilation with a $1° \times 1°$ grid resolution was used. One single backward trajectory (max. 315 h) embedded by ensemble backward trajectories (120 h) are presented for each pollution event. The trajectory ensemble starts multiple trajectories (in total 27) around the starting location. Each member of the trajectory ensemble is calculated by offsetting the meteorological data by a fixed grid factor (one grid meteorological grid point in the horizontal and 0.01 sigma units in the vertical). The altitude of the backward trajectories is expressed by the adjacent color bar. In addition, MODIS (MOderate Resolution Imaging Spectroradiometer) firemaps[5] are shown for the 5-day period prior to the corresponding trajectories in order to assess the influence of biomass burning.

Backward trajectories corresponding to PE1 show near surface air parcels (100 m) originating from northern directions indicating that European and American CO emissions (finding in Sect. 5.2) are transported over northern latitudes towards the Western Pacific. However, high altitude air parcels (2000 m) have their origin further to the west. Transport of pollution from Asia into the Western Pacific is verified. Backward trajectories corresponding to PE2 and starting at 4000 m show that enhanced CO concentrations close to Australia do not have their origin in the Australian continent. Air parcels are transported from the westerly Southern Hemisphere around the continent to the east of Australia. African biomass burning is confirmed to be the major source of the measured CO pollution since MODIS firemaps show strong fires in south-east of Africa during that time period. Backward trajectories corresponding to PE3 and starting at 14 000 m altitude show air parcels to be transported from Indonesia into the Western Pacific. The trajectories start at the Indonesian ground level, are elevated quickly into high altitude, and are then transported into the Western Pacific. Since MODIS firemaps only show a small influence of biomass burning, combustion of fossil fuel is the more likely source of the upper tropospheric CO pollution. PE4 corresponding trajectories starting at 150 m altitude show air parcels coming from the Australian continent, and MODIS firemaps show extensive fire counts in eastern Australia supporting the impact of biomass burning to pollution PE4.

5.3 HCN

Hydrogen cyanide (HCN) is a common tracer for biomass burning emissions with a lifetime of a few months and is

---

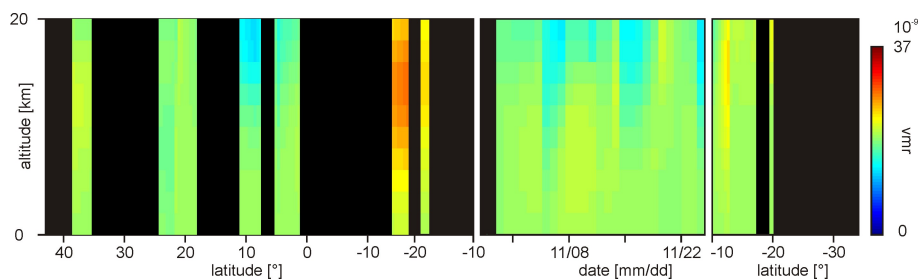[5]http://rapidfire.sci.gsfc.nasa.gov/firemaps/

Fig. 8. HCN profiles retrieved from the solar absorption FTIR measurements during the ship campaign with RV Sonne in the Western Pacific showing the influence of biomass burning emissions on Western Pacific composition.

used to further investigate the influence of biomass burning (Holzinger et al., 1999; Li et al., 2000). HCN profiles derived from solar absorption FTIR measurements are used to investigate this influence on the measured pollution in the Western Pacific during the ship campaign with RV *Sonne*.

In Fig. 8 the HCN profiles derived from the solar absorption FTIR instrument are presented. Information about the retrieval are given in the appendix. Between section S1 and S2 enhanced HCN in the upper troposphere can be found supporting the assignment of air masses influenced by African biomass burning being transported to eastern Australia. A small enhancement in the beginning of cruise section S4 supports the influence of Australian biomass burning to pollution PE4. However, as no further HCN pollution can be determined from Fig. 8, other pollution events are obviously not significantly affected by biomass burning. Particularly, air in the upper troposphere within cruise section S3 is depleted of HCN supporting the finding in Sect. 5.2 that fossil fuel combustion from Indonesia is a major source of upper tropospheric CO pollution in this area.

5.4 Tagged-O$_3$ simulation

In order to verify the source regions of the measured O$_3$ pollution in the Western Pacific, the GEOS-Chem tagged-O$_3$ simulation as described in Sect. 3.3 is used. The tagged-O$_3$ simulation closely reproduces the results from the full-chemistry simulation shown at the top of Fig. 9. Below, Fig. 9 shows the relative contributions of various regions to the total simulated O$_3$ distribution. Since the simulation does not consider secondary production of ozone in the free troposphere from ozone precursors, the contributions of the tagged-tracers are underestimated. However, Fig. 9 provides an overview of the source regions of the measured O$_3$ distribution.

In the Northern Hemisphere, for PE1 the same source regions as identified by the tagged-CO simulation are revealed. Between 43° N and 35° N lower tropospheric pollution originates from European emissions, whereas middle and upper tropospheric pollution mainly originates from North American emissions. Pollution between 35° N and 20° N is caused by Asian emissions. The PE2 pollution in the middle tro-

posphere close to Australia mainly originates from African emissions and South American emissions. Oceanian emissions show a gap in the middle troposphere verifying that Oceanian emissions are not a major source of the observed mid-tropospheric pollution. In cruise section S3 pollution PE3 only originates from Oceanian emissions supporting the conclusion that upper tropospheric pollution mainly originates from Indonesian emissions with small contributions from Oceanian fires as described in Sect. 5.1. In cruise section S4 regarding pollution PE4 Oceanian emissions are the major source. However, between 26° S and 32° S enhanced O$_3$ amounts mainly originate from South American and African emissions.

In the Southern Hemisphere the contributions of African and South American emissions are small. Most of the O$_3$ pollution measured in the Western Pacific from these source regions is, thus, produced during the transport towards the Western Pacific through secondary production from ozone precursors such as CO.

6   Summary and conclusions

In this study we have reported about the first measurements of CO and O$_3$ in the Western Pacific performed with solar absorption Fourier Transform infrared spectrometry during a ship campaign with RV *Sonne* in fall 2009. In-situ observations from three different instruments have also contributed to this study.

The observations have been compared to the 3-D chemistry transport model GEOS-Chem showing that the model generally reproduces CO and O$_3$ concentrations well. The carbon monoxide variability is clearly expressed by the model, however, absolute values are underestimated due to a constant low bias in the simulation already known from previous studies. In the beginning of the campaign, in mid latitudes CO surface concentrations were largely overestimated by the model. Here, the model seems to mix free tropospheric air into the boundary layer too readily. Ozone concentrations were outstandingly reproduced by the GEOS-chem model during the entire ship campaign both in magnitude and variability.
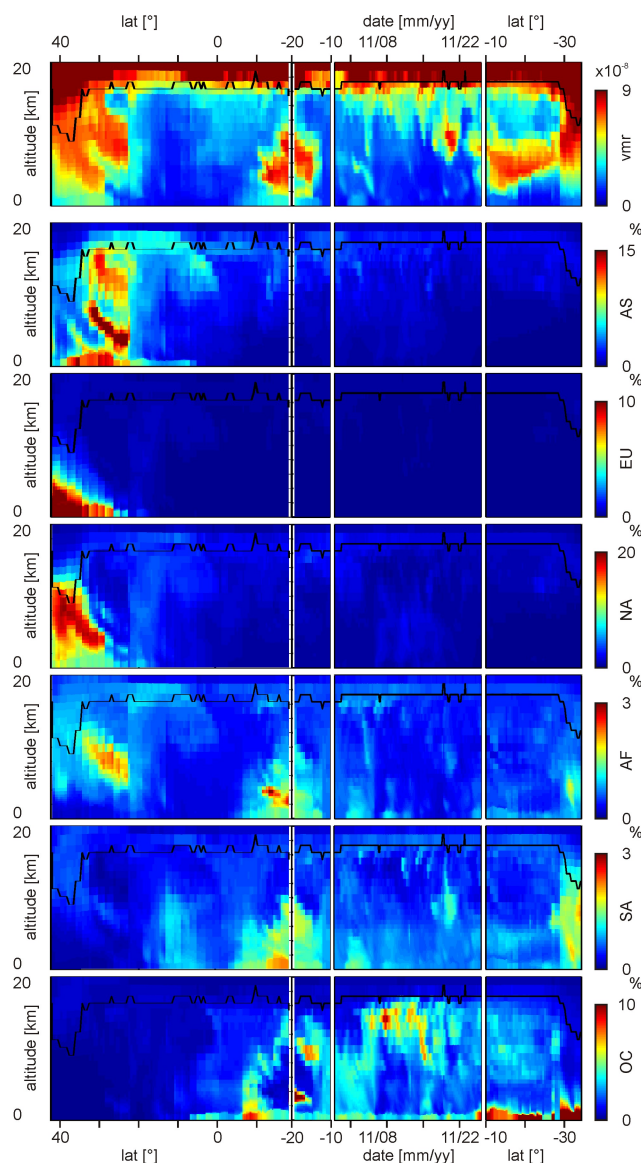
Fig. 9. Relative contributions of various GEOS-Chem tagged regions to the measured O$_3$ pollution calculated with the tagged-O$_3$ simulation. AS: Asia, EU: Europe, NA: North America, AF: Africa, SA: South America, OC: Oceania. The black line in each graph indicates the model tropopause height.

The variability of the CO and O$_3$ distributions is largely similar suggesting impacts from similar source regions. This is verified with a subjective assessment of the source processes and source regions of the measured CO and O$_3$ pollution using tagged tracer simulations, MODIS firemaps, HYSPLIT trajectory calculations, and solar absorption FTIR measurements of HCN.

Large parts of the West Pacific belong to Earth's most remote areas. While much of the air observed in this region is considered the cleanest air world wide, the presented observations show the presence of distinct plumes of elevated car-

bon monoxide and ozone. Trajectory based transport studies and studies with a full chemical transport model show that the cause of this pollution is global scale transport of pollutants with contributions from source regions as far away as Europe.

The analysis of several different carbon monoxide and ozone pollution events sampled during the RV *Sonne* ship campaign has demonstrated that in the Northern Hemisphere the main contributor to Western Pacific tropospheric air pollution is Asian fossil fuel combustion. Contributions from European emissions and North American emissions in the lower and middle troposphere are significant as well.

In the Southern Hemisphere biomass burning and fossil fuel combustion are determined to cause carbon monoxide and ozone pollution observed during the RV *Sonne* ship campaign. In particular, African and South American biomass burning significantly contribute to Western Pacific air pollution. Fossil fuel combustion in Indonesia is a major contribution to upper tropospheric pollution in the tropical Western Pacific. This pollution within the tropical tropopause layer is transported by radiative heating into the stratosphere and has an impact on stratospheric composition.

The presented analysis provides a detailed evaluation of the source processes and source regions of Western Pacific carbon monoxide and ozone pollution measured during a ship campaign from Japan to New Zealand in fall 2009. Thus, the analysis is limited on the abovementioned period ob time. In order to obtain a better knowledge of Western Pacific air contamination, future measurements in this region with high temporal and spatial resolution are needed as they are currently performed by, for example, the HIAPER Pole to Pole Observation (HIPPO) aircraft campaign (Wofsy, 2011) and the SHIVA (Stratospheric ozone: Halogen Impacts in a Varying Atmosphere) campaign.

Appendix A

HCN retrieval

In Fig. 8 the solar absorption FTIR profiles of HCN during the ship campaign with RV *Sonne* were shown. HCN was simultaneously fitted in four microwindows ($3268.1800\,\mathrm{cm}^{-1}$–$3268.2700\,\mathrm{cm}^{-1}$, $3287.1800\,\mathrm{cm}^{-1}$–$3287.3200\,\mathrm{cm}^{-1}$, $3299.4600\,\mathrm{cm}^{-1}$–$3299.5800\,\mathrm{cm}^{-1}$, $3305.4000\,\mathrm{cm}^{-1}$–$3305.7000\,\mathrm{cm}^{-1}$) with H$_2O, C_2H_2$, and CO$_2$ also fitted as interfering gases. HCN reaches a DOF of around 2 with the main sensitivity in the upper troposphere. The corresponding averaging kernels are presented in Fig. A1.
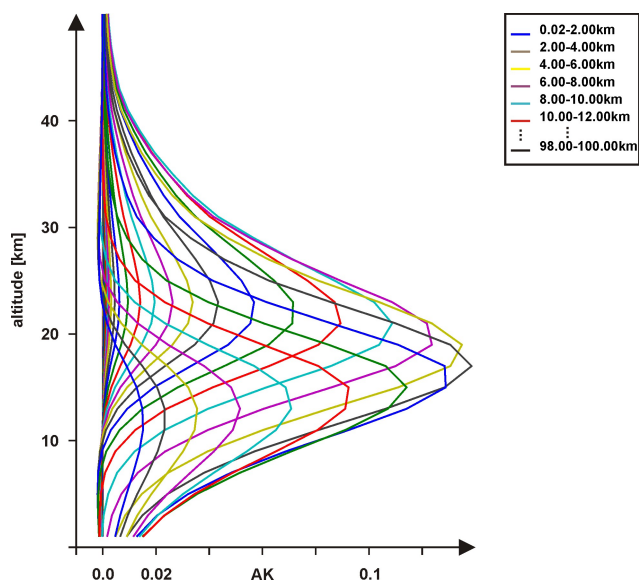
Fig. A1. Representative averaging kernels of the FTIR HCN retrieval. The colored lines indicate the sensitivity and resolution of each individual layer.

Edited by: K. Krueger

References

Andreae, M. O., Artaxo, P., Fischer, H., Freitas, S. R., Grégoire, J.-M., Hansel, A., Hoor, P., Kormann, R., Krejci, R., Lange, L., Lelieveld, J., Lindinger, W., Longo, K., Peters, W., de Reus, M., Scheeren, B., Silva Dias, M. A. F., Ström, J., van Velthoven, P. F. J., and Williams, J.: Transport of biomass burning smoke to the upper troposphere by deep convection in the equatorial region, Geophys. Res. Lett., 28, 951–954, doi:10.1029/2000GL012391, 2001.

Bey, I., Jacob, D. J., Logan, J. A., and Yantosca, R. M.: Asian chemical outflow to the Pacific in spring: Origins, pathways, and budgets, J. Geophys. Res., 106, 23097–23113, doi:10.1029/2001JD000806, 2001a.

Bey, I., Jacob, D. J., Yantosca, R. M., Logan, J. A., Field, B. D., Fiore, A. M., Li, Q., Liu, H. Y., Mickley, L. J., and Schultz, M. G.: Global modeling of tropospheric chemistry with assimilated meteorology: Model description and evaluation, J. Geophys. Res., 106, 23073–23095, doi:10.1029/2001JD000807, 2001b.

Draxler, R. R. and Hess, G. D.: Description of the HYSPLIT4 modeling system, NOAA Tech. Memo. ERL ARL-224, NOAA Air Resources Laboratory, 24 pp., 1997.

Draxler, R. R. and Hess, G. D.: An overview of the HYSPLIT4 modeling system of trajectories, dispersion, and deposition, Aust. Meteorol. Mag., 47, 295–308, 1998.

Duncan, B. N., Logan, J. A., Bey, I., Megretskaia, I. A., Yantosca, R. M., Novelli, P. C., Jones, N. B., and Rinsland, C. P.: Global budget of CO, 1988–1997: Source estimates and validation with a global model, J. Geophys. Res., 112, D22301, doi:10.1029/2007JD008459, 2007.

Esler, M. B., Griffith, D. W. T., Wilson, S. R., and Steele, L. P.: Precision Trace Gas Analysis by FT-IR Spectroscopy, 1. Simultaneous Analysis of CO$_2$, CH$_4$, N$_2$O, and CO in Air, Anal. Chem., 72, 206–215, doi:10.1021/ac9905625, 2000.

Fueglistaler, S., Wernli, H., and Peter, T.: Tropical troposphere-to-stratosphere transport inferred from trajectory calculations, J. Geophys. Res., 109, D03108, doi:10.1029/2003JD004069, 2004.

Fueglistaler, S., Dessler, A. E., Dunkerton, T. J., Folkins, I., Fu, Q., and Mote, P. W.: Tropical tropopause layer, Rev. Geophys., 47, RG1004, doi:10.1029/2008RG000267, 2009.

Garcia, R. R., Marsh, D. R., Kinnison, D. E., Boville, B. A., and Sassi, F.: Simulation of secular trends in the middle atmosphere, 1950–2003, J. Geophys. Res., 112, D09301, doi:10.1029/2006JD007485, 2007.

Griffith, D., Deutscher, N., Krummel, P. Fraser, P., van der Schoot, M., and Allison, C.: The UoW FTIR trace gas analyser: comparison with LoFlo, AGAGE and tank measurements at Cape Grim and GASLAB, in: Baseline Atmospheric Program (Australia) 2007–2008, edited by: Derek, N. and Krummel, P. B., Australian Bureau of Meteorology and CSIRO Marine and Atmospheric Research, Melbourne, Australia, 7–22, 2011.

Griffith, D. W.: FT-IR Measurements of Atmospheric Trace Gases and their Fluxes, John Wiley & Sons, Ltd, doi:10.1002/0470027320.s6802, 2002.

Griffith, D. W. T.: Synthetic Calibration and Quantitative Analysis of Gas-Phase FT-IR Spectra, Appl. Spectrosc., 50, 59–70, 1996.

Holton, J. R., Haynes, P. H., McIntyre, M. E., Douglass, A. R., Rood, R. B., and Pfister, L.: Stratosphere-troposphere exchange, Rev. Geophys., 33, 403–439, doi:10.1029/95RG02097, 1995.

Holzinger, R., Warneke, C., Hansel, A., Jordan, A., Lindinger, W., Scharffe, D. H., Schade, G., and Crutzen, P. J.: Biomass burning as a source of formaldehyde, acetaldehyde, methanol, acetone, acetonitrile, and hydrogen cyanide, Geophys. Res. Lett., 26, 1161–1164, doi:10.1029/1999GL900156, 1999.

Jacob, D. J., Crawford, J. H., Kleb, M. M., Connors, V. S., Bendura, R. J., Raper, J. L., Sachse, G. W., Gille, J. C., Emmons, L., and Heald, C. L.: Transport and Chemical Evolution over the Pacific (TRACE-P) aircraft mission: Design, execution, and first results, J. Geophys. Res., 108, 9000, doi:10.1029/2002JD003276, 2003.

Jaeglé, L., Jaffe, D. A., Price, H. U., Weiss-Penzias, P., Palmer, P. I., Evans, M. J., Jacob, D. J., and Bey, I.: Sources and budgets for CO and O$_3$ in the northeastern Pacific during the spring of 2001: Results from the PHOBEA-II Experiment, J. Geophys. Res., 108, 8802, doi:10.1029/2002JD003121, 2003.

Kopacz, M., Jacob, D. J., Fisher, J. A., Logan, J. A., Zhang, L., Megretskaia, I. A., Yantosca, R. M., Singh, K., Henze, D. K., Burrows, J. P., Buchwitz, M., Khlystova, I., McMillan, W. W., Gille, J. C., Edwards, D. P., Eldering, A., Thouret, V., and Nedelec, P.: Global estimates of CO sources with high resolution by adjoint inversion of multiple satellite datasets (MOPITT, AIRS, SCIAMACHY, TES), Atmos. Chem. Phys., 10, 855–876,

doi:10.5194/acp-10-855-2010, 2010.

Krüger, K. and Quack, B.: Introduction to special issue: the TransBrom Sonne expedition in the tropical West Pacific, Atmos. Chem. Phys. Discuss., 12, 1401–1418, doi:10.5194/acpd-12-1401-2012, 2012.

Krüger, K., Immler, F., Tegtmeier, S., Fuhlbrügge, S., Mohr, V., Wache, S., Rex, M., and Quack, B.: High resolution radiosonde data above the tropical West Pacific, Atmos. Chem. Phys. Discuss., in preparation, 2012.

Kurylo, M. J.: Network for the detection of stratospheric change (NDSC), in: Society of Photo-Optical Instrumentation Engineers (SPIE) Conference Series, edited by: McElroy, J. L. and McNeal, R. J., vol. 1491 of Society of Photo-Optical Instrumentation Engineers (SPIE) Conference Series, 168–174, 1991.

Li, Q., Jacob, D. J., Bey, I., Yantosca, R. M., Zhao, Y., Kondo, Y., and Notholt, J.: Atmospheric hydrogen cyanide (HCN): Biomass burning source, ocean sink?, Geophys. Res. Lett., 27, 357–360, doi:10.1029/1999GL010935, 2000.

Li, Q., Jacob, D. J., Bey, I., Palmer, P. I., Duncan, B. N., Field, B. D., Martin, R. V., Fiore, A. M., Yantosca, R. M., Parrish, D. D., Simmonds, P. G., and Oltmans, S. J.: Transatlantic transport of pollution and its effects on surface ozone in Europe and North America, J. Geophys. Res., 107, 4166, doi:10.1029/2001JD001422, 2002.

Liu, H., Jacob, D. J., Chan, L. Y., Oltmans, S. J., Bey, I., Yantosca, R. M., Harris, J. M., Duncan, B. N., and Martin, R. V.: Sources of tropospheric ozone along the Asian Pacific Rim: An analysis of ozonesonde observations, J. Geophys. Res., 107, 4573, doi:10.1029/2001JD002005, 2002.

Notholt, J., Toon, G. C., Rinsland, C. P., Pougatchev, N. S., Jones, N. B., Connor, B. J., Weller, R., Gautrois, M., and Schrems, O.: Latitudinal variations of trace gas concentrations in the free troposphere measured by solar absorption spectroscopy during a ship cruise, J. Geophys. Res., 105, 1337–1349, doi:10.1029/1999JD900940, 2000.

Notholt, J., Kuang, Z., Rinsland, C. P., Toon, G. C., Rex, M., Jones, N., Albrecht, T., Deckelmann, H., Krieg, J., Weinzierl, C., Bingemer, H., Weller, R., and Schrems, O.: Enhanced Upper Tropical Tropospheric COS: Impact on the Stratospheric Aerosol Layer, Science, 300, 307–310, doi:10.1126/science.1080320, 2003.

Notholt, J., Luo, B. P., Fueglistaler, S., Weisenstein, D., Rex, M., Lawrence, M. G., Bingemer, H., Wohltmann, I., Corti, T., Warneke, T., von Kuhlmann, R., and Peter, T.: Influence of tropospheric SO$_2$ emissions on particle formation and the stratospheric humidity, Geophys. Res. Lett., 32, L07810, doi:10.1029/2004GL022159, 2005.

Palm, M., v. Savigny, C., Warneke, T., Velazco, V., Notholt, J., Künzi, K., Burrows, J., and Schrems, O.: Intercomparison of O$_3$ profiles observed by SCIAMACHY and ground based microwave instruments, Atmos. Chem. Phys., 5, 2091–2098, doi:10.5194/acp-5-2091-2005, 2005.

Quack, B. and Krüger, K.: Cruise Report TransBrom SONNE, Berichte aus dem Leibniz-Institut für Meereswissenschaften an der Christian-Albrechts-Universität zu Kiel, 37, 1–86, 2010.

Rao, K. N.: Spectroscopy of the Earth's Atmosphere and Interstellar Medium, Academic Press, Boston, USA, 1–536, 1992.

Ridder, T., Warneke, T., and Notholt, J.: Source brightness fluctuation correction of solar absorption fourier transform mid infrared spectra, Atmos. Meas. Tech., 4, 1045–1051, doi:10.5194/amt-4-1045-2011, 2011.

Rienecker, M. M., Suarez, M. J., Todling, R., Bacmeister, J., Takacs, L., Liu, H.-C., Gu, W., Sienkiewicz, M., Koster, R. D., Gelaro, R., Stajner, I., and Nielsen, J. E.: The GEOS-5 Data Assimilation System – Documentation of Versions 5.0.1, 5.1.0, and 5.2.0, Technical Report Series on Global Modeling and Data Assimilation, 27, NASA/TM–2007–104606, 2008.

Rinsland, C. P., Jones, N. B., Connor, B. J., Logan, J. A., Pougatchev, N. S., Goldman, A., Murcray, F. J., Stephen, T. M., Pine, A. S., Zander, R., Mahieu, E., and Demoulin, P.: Northern and southern hemisphere ground-based infrared spectroscopic measurements of tropospheric carbon monoxide and ethane, J. Geophys. Res., 103, 28197–28217, doi:10.1029/98JD02515, 1998.

Rodgers, C. D.: Characterization and Error Analysis of Profiles Retrieved From Remote Sounding Measurements, J. Geophys. Res., 95, 5587–5595, doi:10.1029/JD095iD05p05587, 1990.

Rodgers, C. D.: Inverse Methods for Atmospheric Sounding: Theory and Practice, World Scientific Publishing Company, London, UK, 1–240, 2000.

Rodgers, C. D. and Connor, B. J.: Intercomparison of remote sounding instruments, J. Geophys. Res., 108, 4116, doi:10.1029/2002JD002299, 2003.

Sauvage, B., Martin, R. V., van Donkelaar, A., and Ziemke, J. R.: Quantification of the factors controlling tropical tropospheric ozone and the South Atlantic maximum, J. Geophys. Res., 112, D11309, doi:10.1029/2006JD008008, 2007.

Schneider, M., Hase, F., Blumenstock, T., Redondas, A., and Cuevas, E.: Quality assessment of O$_3$ profiles measured by a state-of-the-art ground-based FTIR observing system, Atmos. Chem. Phys., 8, 5579–5588, doi:10.5194/acp-8-5579-2008, 2008.

Solomon, S., Qin, D., Manning, M., Chen, Z., Marquis, M., Averyt, K. B., Tignor, M., and Miller, H. L.: Climate Change 2007: The Physical Science Basis. Contribution of Working Group I to the Fourth Assessment Report of the Intergovernmental Panel on Climate Change, Cambridge University Press, Cambridge, UK and New York, NY, USA, 2007.

Staudt, A. C., Jacob, D. J., Logan, J. A., Bachiochi, D., Krishnamurti, T. N., and Sachse, G. W.: Continental sources, transoceanic transport, and interhemispheric exchange of carbon monoxide over the Pacific, J. Geophys. Res., 106, 32571–32589, doi:10.1029/2001JD900078, 2001.

Thompson, A. M., Witte, J. C., Hudson, R. D., Guo, H., Herman, J. R., and Fujiwara, M.: Tropical Tropospheric Ozone and Biomass Burning, Science, 291, 2128–2132, doi:10.1126/science.291.5511.2128, 2001.

Velazco, V., Notholt, J., Warneke, T., Lawrence, M., Bremer, H., Drummond, J., Schulz, A., Krieg, J., and Schrems, O.: Latitude and altitude variability of carbon monoxide in the Atlantic detected from ship-borne Fourier transform spectrometry, model, and satellite data, J. Geophys. Res., 110, D09306, doi:10.1029/2004JD005351, 2005.

Warneke, T., Meirink, J. F., Bergamaschi, P., Grooß, J.-U., Notholt, J., Toon, G. C., Velazco, V., Goede, A. P. H., and Schrems, O.: Seasonal and latitudinal variation of atmospheric methane: A ground-based and ship-borne solar IR spectroscopic study, Geophys. Res. Lett., 33, L14812, doi:10.1029/2006GL025874, 2006.

White, J. U.: Long Optical Paths of Large Aperture, J. Opt. Soc.

Am., 32, 285, doi:10.1364/JOSA.32.000285, 1942.

Wofsy, S. C.: HIAPER Pole-to-Pole Observations (HIPPO): fine-grained, global-scale measurements of climatically important atmospheric gases and aerosols, Phil. Trans. R. Soc. A, 369, 2073–2086, doi:10.1098/rsta.2010.0313, 2011.

Wunch, D., Toon, G. C., Blavier, J.-F. L., Washenfelder, R. A., Notholt, J., Connor, B. J., Griffith, D. W. T., Sherlock, V., and Wennberg, P. O.: The Total Carbon Column Observing Network, Philos. T. Roy. Soc. A, 369, 2087–2112, doi:10.1098/rsta.2010.0240, 2011.

Yan, X.-H., Ho, C.-R., Zheng, Q., and Klemas, V.: Temperature and Size Variabilities of the Western Pacific Warm Pool, Science, 258, 1643–1645, doi:10.1126/science.258.5088.1643, 1992.

Zhang, L., Jacob, D. J., Boersma, K. F., Jaffe, D. A., Olson, J. R., Bowman, K. W., Worden, J. R., Thompson, A. M., Avery, M. A., Cohen, R. C., Dibb, J. E., Flock, F. M., Fuelberg, H. E., Huey, L. G., McMillan, W. W., Singh, H. B., and Weinheimer, A. J.: Transpacific transport of ozone pollution and the effect of recent Asian emission increases on air quality in North America: an integrated analysis using satellite, aircraft, ozonesonde, and surface observations, Atmos. Chem. Phys., 8, 6117–6136, doi:10.5194/acp-8-6117-2008, 2008.